Non-invasive visualization of cortical columns by fMRI

Amiram Grinvald, Hamutal Slovin and Ivo Vanzetta

Functional magnetic resonance imaging can now resolve individual cortical columns, which should provide insights into sensory perception and higher cognitive functions.

Mountcastle[1] and Hubel and Wiesel[2] originally showed that many complex neural networks display meticulous order. Neurons with common functional properties are often clustered together in columns, 200–1000 μm wide, which span the depth of the cortex. To discover principles underlying implementation of the 'neural code', we must understand functional organization across the sheet of cortical columns during sensory processing and cognitive tasks. Brain organization has been visualized[3] with positron-emission tomography (PET), optical imaging of intrinsic signals and, most recently, functional magnetic resonance imaging (fMRI). Optical imaging allows detailed visualization of cortical columns (spatial resolution of 20–100 μm, verified by extensive single-neuron and histological mapping), but it is invasive and thus unsuitable for use in humans. PET and fMRI offer spectacular three-dimensional localization of activity in humans, but have lacked the spatial resolution to reveal cortical columns.

These techniques depend on the pioneering finding of Roy and Sherrington[4] that changes in electrical activity are coupled to microcirculation responses, whose regulation is still being explored. Neural activity locally increases metabolic demands for glucose and oxygen, and the brain microcirculation responds—much less locally—by increasing blood volume and flow. In PET, this enhanced blood flow is visualized by injecting radioactive material into the circulation. Blood oxygenation level-dependent[5] (BOLD) fMRI instead uses concentration changes in paramagnetic deoxygenated hemoglobin as an intrinsic contrast agent. In optical imaging, this contrast agent yields high-resolution maps of cortical columns[6,7], and BOLD imaging was hoped to have similar potential. Kim and colleagues[8] now report a striking technical advance in fMRI, achieving sufficient spatial resolution to directly visualize cortical columns responsible for shape perception in visual cortex of anesthetized cats. Instead of the traditional positive BOLD fMRI signal, the authors used an earlier, negative phase of the signal, termed the 'initial dip' (deoxygenation phase; Fig. 1b in ref. 8), to obtain single-condition maps of cortical columns. They further showed that the traditional BOLD signal (positive hyperoxygenation phase) gives less precise resolution than this early phase.

Because it remains controversial exactly how electrical activity is coupled to such metabolic responses, skeptics question whether imaging maps based on microcirculation responses indeed represent the brain's electrical activity or just hemodynamics. Thus methods to distinguish between 'brain and vein'[9] are critical. After Kim and colleagues presented their results[8] at the 1999 Society for Neuroscience meeting, some felt that neuroscientists' fantasy might soon become reality. For others, questions remained. Exactly how is cortical electrical activity related to various hemodynamic responses? Why was the initial dip not observed in most previous studies? What are the implications for standard low-resolution fMRI at low field strength? Can the impressive single-condition orientation columns obtained by fMRI in the anesthetized cat also be visualized in awake animals? Are these results relevant to primates?

The relationship of electrical activity to hemodynamic responses has been addressed by optical imaging[6,7,10,11]. Because the spatial resolution of the optics is less than 1 μm, this method permits unambiguous identification of blood-vessel-derived artifacts, distinguishing them from cortical activation *per se*. In addition, photons are cheap, so one can collect plenty of them; thus the signal-to-noise ratio is higher than for fMRI. This allows direct visualization of hemodynamic changes without elaborate image processing or statistics. Below we address these five remaining questions by presenting our own optical imaging data showing ocular dominance columns in behaving monkeys (**Figs. 1** and **2**) and by referring to previous work using biophysics and optical imaging.

We determined the activity-dependent spatiotemporal characteristics of hemodynamic events, including oxygen delivery, blood flow and blood volume, at the onset of cortical activity triggered by sensory stimulation. The first event is a prolonged increase in oxygen consumption, caused by an increase in oxidative metabolism of activated neurons, leading to an increase in the deoxyhemoglobin concentration starting less than 100 ms after activity onset[10,11]. Upon illumination at 605 nm, this early event causes cortical darkening (**Figs. 1b,** middle panel, and **2b**) known to be colocalized with the site of electrical activity in columns (see Fig. 4 in ref. 7). The second event originates from a delayed increase in blood volume, starting about 300–500 ms later[10], caused by capillary dilation, which also causes cortical darkening, particularly apparent in larger blood vessels (**Figs. 1c** and **d,** middle panel, and **2e**). Blood volume changes occur almost simultaneously in the three vascular compartments and are not well regulated within individual cortical columns (Fig. 4 in ref. 7). The third event is an activity-related increase in blood flow, as blood rushes into capillaries. Starting about 0.5–1.5 seconds after the onset of electrical activity, this decreases deoxyhemoglobin concentration and increases oxyhemoglobin concentration. The delayed deoxyhemoglobin decrease is much larger than the initial increase, causing delayed cortical whitening, particularly apparent in larger blood vessels (**Fig. 1b** and **c**, right). Unlike the early deoxygenation phase, this delayed increase is not localized with columnar electrical activity. Thus, changes in deoxyhemoglobin concentration follow a biphasic time course: a deoxyhemoglobin increase because of increased oxidative metabolism of active neurons — the initial dip — and then a decrease due to large overcompensation by enhanced blood flow (**Figs. 1b** and **2b**). Obviously, increased oxidative metabolism must localize with electrical activity.

With high-field fMRI, Logothetis and colleagues[12] observed the initial dip in cortical regions without large vessels but not in large vessels, whereas the late BOLD component was detectable in both compartments (see Fig. 5 in ref. 12). These findings support the claims of Kim and colleagues[8] that the initial fMRI dip shows better spatial specificity. Thus, cortical

The authors are in the Department of Neurobiology, The Weizmann Institute of Science, Rehovot 76100, Israel.
e-mail: amiram.grinvald@weizmann.ac.il

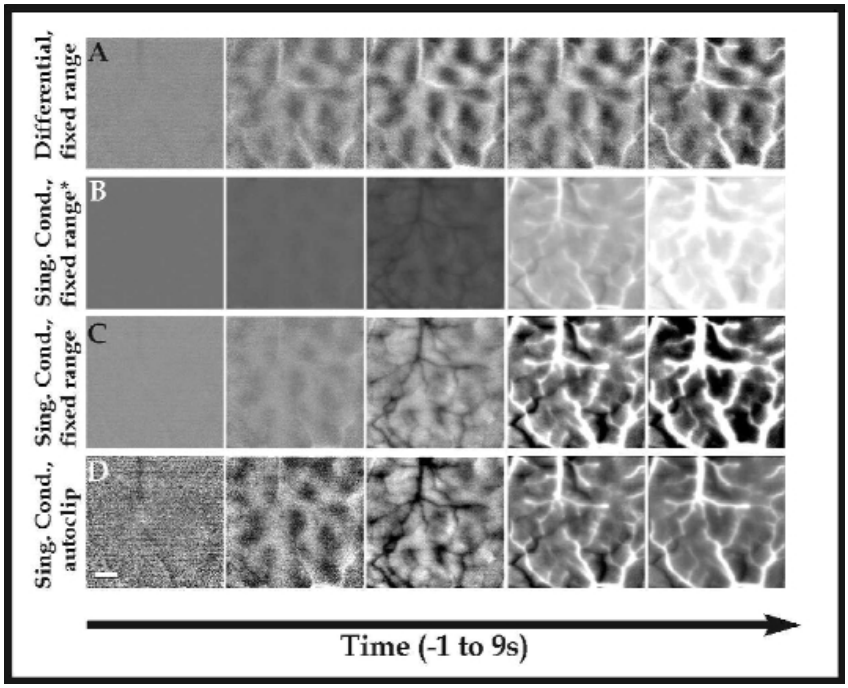

Fig. 1. Comparison between differential and single-condition maps of ocular dominance columns, visualized by optical imaging. A cranial window was implanted over the primary visual cortex of a macaque. The exposed cortical surface of the behaving monkey was illuminated at 605 nm to emphasize small changes in deoxyhemoglobin concentration. Each row represents a time series, taken at roughly two-second intervals beginning one second before stimulus onset. (**a**) Differential images, obtained by subtracting images obtained with left- versus right-eye stimulation. To show time development of the differential map, all images are clipped at the same range. (Clipping is determining the range and mean of the gray scale's contrast.) (**b**) Corresponding single-condition maps obtained by normalizing the cortical image to illumination intensity without any additional processing, when the contralateral eye viewed the stimulus. To emphasize the slow global changes, a fixed-range clipping with fixed mean values was used. (**c**) As in (**b**), but to emphasize the small changes, a fixed range was used without a fixed mean. (**d**) As for (**b**), but to maximize the dynamic range of each map, autoclipping was used. Note that the signal-to-noise ratio in a differential image is much higher than that obtained for a single-condition map. Scale bar, 1 mm.

electrical activity is most tightly coupled to hemodynamic events during the initial dip. Because the initial dip is localized with neuronal activity, whereas the subsequent larger decrease in deoxyhemoglobin is not, there is a time window during the first three or four seconds in which functional maps indeed correspond to electrical activity. In contrast, delayed microvascular events such as volume and flow changes, which are not localized with electrical activity, may yield 'hemodynamic maps' that do not correspond to electrical activation (compare **Fig. 2g** and **h** with Figs. 3a and b and 4c in ref. 8).

Why have low-field (0.5–1.5 T) BOLD fMRI measurements failed to detect the initial dip observed by Kim and colleagues with high-field (4.7 T and 9.4 T) magnets and by optical imaging? One possibility is that low-field measurements are not sufficiently sensitive to deoxyhemoglobin concentration changes in cortical capillaries. Both theoretical and experimental evidence suggest that the amplitude of the initial dip depends on the second power of the field strength (K. Ugurbil, personal communication). The existence of the initial dip has been confirmed by several groups using 4 T fMRI in humans[13]. For those debating whether to purchase ultra-expensive high-field magnets, it will be critical to establish the relative amplitude and signal-to-noise ratio of the initial dip as a function of field strength.

Kim and colleagues reported single-condition maps (Fig. 2a–d in ref. 8). To understand the implications of their advance for standard low-field fMRI research (the third question), we must clarify the advantages and limitations of 'single-condition mapping' compared with 'differential mapping' (for details, see ref. 3, pages 918–921). The spatial resolution of a functional map depends on the spread of a particular imaged signal beyond the site of electrical activity, signal-to-noise ratio and the instrument's spatial resolution. The point spread of the fMRI signal is large relative to cortical column diameter[14]. However, differential imaging can resolve two distinct cortical activation sites at distances much smaller than half the width of the signal spread, if the signal-to-noise ratio is adequate. Indeed, ocular dominance columns in humans have already been imaged with fMRI by this method[15] (see also T.W. James *et al. Soc. Neurosci. Abstr.* **25**, 212.5,1999; Tanaka *et al.*, *Soc. Neurosci. Abstr.* **25**, 572.3, 1999). As discussed above, both optical imaging and BOLD fMRI signals have multiple components. The 'local' component probably originates from oxygen extraction from the capillaries; thus it is most closely coupled to electrical activity and most stimulus-specific. This component is particularly enhanced during the initial dip, before delayed hemodynamic events begin to obscure it. The global signal[7,10] refers to the sum of all the components, which originate from this deoxygenation and other sources, such as nonlocalized blood-volume and blood-flow changes (black and white vessels, respectively, in **Fig. 1a–d**, late frames). Most of the integrated global signal is associated with these last two components, which may not be stimulus-specific as they reflect hemodynamic activation of venules and large draining veins far from the electrical activation site[7,10]. For this reason, when two stimuli are orthogonal—meaning that they activate neurons in complementary cortical patches—comparing their activation patterns enhances the signal's local component, while eliminating many, though not all, global components.

Therefore, when the assumptions discussed below are fully justified, differential imaging may reveal the correct pattern of electrical activation. Such maps may even yield a better signal-to-noise ratio than maps derived from the shorter period and smaller amplitude of the initial dip. However, differential imaging has two major limitations. First, it works perfectly only if stimuli are orthogonal in the above sense, such as orthogonal oriented stimuli activating orientation columns in cats and monkeys. Even for ocular dominance maps, the stimuli are not strictly orthogonal because contralateral activation is stronger than ipsilateral activation, so that blood vessel-derived artifacts may be the largest signals in differential maps computed from late hemodynamic responses (**Fig. 2c** and compare early vascular artifacts in **Fig. 2f** with late ones in **Fig. 2i**). More generally, functional map

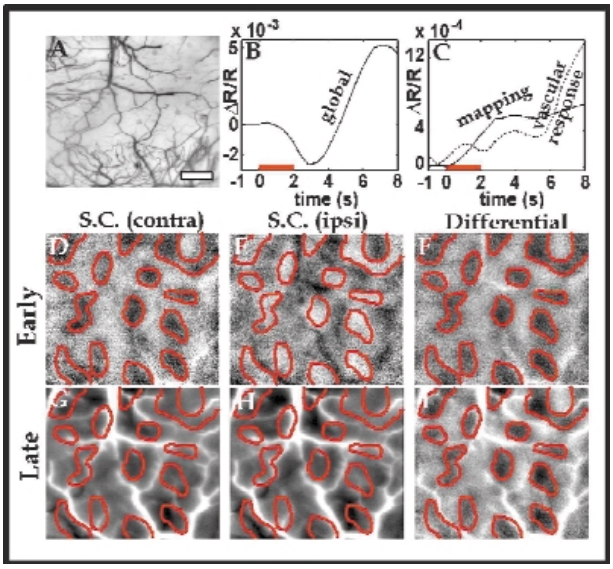

Fig. 2. Comparison between single-condition and differential maps obtained during the initial dip (deoxygenation phase) and later rise (hyperoxygenation phase). (**a**) Cortical image taken in green light to emphasize the vascular pattern. Scale bar, 1 mm. (**b**) Time course of the amplitude of the global signal obtained from the single-condition maps. (**c**) Time course of vascular artifacts and of the mapping signal amplitude calculated from the differential map. (**d**–**f**) Maps from the early deoxygenation phase. (**d**) Single-condition map for the contralateral eye. (**e**) As in (**d**), for the ipsilateral eye. (**f**) The differential map. (**g**–**i**) As for (**d**–**f**), from the late period. Note that during this late time, the most prominent signals in the rather poor single-condition maps (**g**, **h**) are artifacts from blood vessels (diameter 50–150 μm). Although these 'brain or vein' artifacts are minimized by differential mapping (**f**), at least with optical imaging, they are larger than the columnar signal.

amplitudes can be three- to tenfold smaller than ocular dominance column maps shown here, making vessel-derived artifacts far more problematic. Furthermore, orthogonal stimuli may be impossible to design, particularly for columns representing higher cognitive functions. Second, by far the largest signals are from draining veins, even those smaller than 100 μm (cortical vasculature image, **Fig. 2a**; vascular artifacts **Fig. 2c** and **g**–**i**). Such large signals may spread 3–7 mm from the sites of electrical activity (A. Shmuel *et al.*, ISMRM abstract, in press; D. Shoham and A.G., unpublished results). Most important, signals from such draining veins may be stimulus-specific and highly reproducible. Therefore, use of differential imaging, high thresholds, signal averaging and statistics does not guarantee removal of such artifacts. Single-condition mapping, in which the response to a single stimulus is imaged directly, thus has great advantages over differential imaging and should be the ultimate goal of high-resolution functional brain imaging.

Finally, skeptics wondered whether single-condition orientation columns obtained in anesthetized cats[8] can be visualized in awake animals, and whether these results are relevant to primates. Our new results from awake monkey cortex (**Figs. 1** and **2**), which agree with those of Kim and colleagues[8], address both these concerns. Hence it seems reasonable to hope that human brain imaging with fMRI will also allow high-resolution single-condition mapping.

Kim and colleagues accomplished the difficult feat of single-condition mapping by integrating BOLD signals mainly during the small initial dip. As with any new approach, additional research will undoubtedly strengthen this work's foundations. First, the authors did not present unequivocal single-neuron confirmation, or confirmation by two-deoxyglucose autoradiography or optical imaging, which would be even better. However, the complementary nature of the single-condition maps for the two sets of orthogonal orientations strongly suggests that their maps were indeed orientation maps. Second, their choice of threshold, a critical step in obtaining single-condition maps, was arbitrary. A 'cocktail blank' (average response to four stimuli, a rough approximation for uniform cortical activation elicited by many stimuli) was used instead of a real blank (no stimulus). Third, one would expect a small negative BOLD signal also for the orthogonal orientation, rather than a flat line or a small positive signal (**Fig. 2e** and **f** in ref. 8). This last reservation may suggest that current signal-to-noise ratio is not good enough yet. Such single-condition mapping is difficult even with optical imaging. (Cocktail blanks are commonly used in optical imaging studies as well[3].) Therefore, future work should emphasize increasing signal-to-noise ratio, and additional technical improvements are still required before high-resolution single-condition mapping becomes a 'gold standard' procedure easily achieved by fMRI. Such improvements might include extensive averaging, use of different MRI sequences, improved ways to reject vascular artifacts or reliance on MRI signals other than BOLD.

The advance described by Kim and colleagues[8] represents a major step forward in functional brain imaging. It should lay the foundation for exploration of the human brain at the fundamental level of its columnar architecture. This approach may revolutionize fMRI studies by allowing them to address not only where but also how processing and computations are carried out by individual cortical columns. The combination of fMRI with techniques that reveal cortical dynamics in the millisecond time domain, such as electroencephalography and magnetoencephalography, is also warranted. In conjunction with such methods, fMRI will become a powerful non-invasive tool both in biomedicine and in basic research of neurophysiology underlying higher brain functions, thus bridging the gap between psychology and neurobiology.

1. Mountcastle, V. B. *J. Neurophysiol.* **20**, 408–434 (1957).
2. Hubel, D. H. & Wiesel, T. N. *J. Physiol. (Lond.)* **160**, 106–154 (1962).
3. Windhorst, U. & Johansson, H. (eds) *Modern Techniques in Neuroscience Research* (Springer, New York, 1999).
4. Roy, C. & Sherrington, C. *J. Physiol (Lond.).* **11**, 85-108 (1890).
5. Ogawa, S., Lee, T. M., Kay, A. R. & Tank, D. W. *Proc. Natl. Acad. Sci. USA* **87**, 9868–9872 (1990).
6. Grinvald, A., Lieke, E., Frostig, R. D, Gilbert, C. D. & Wiesel, T. N. *Nature* **324**, 361–364 (1986).
7. Frostig R. D., Lieke, E., Ts'o, D. Y. & Grinvald, A. *Proc. Natl. Acad. Sci. USA* **87**, 6082–6086 (1990).
8. Kim, D.-S., Duong, T. Q. & Kim, S.-G. *Nat. Neurosci.* **3**, 164–169 (2000).
9. Frahm, J. Merboldt, K. D., Hanike, W., Kleinschmisdt, A. & Boeker, H. *NMR Biomed.* **7**, 45–53 (1994).
10. Malonek, D. & Grinvald, A. *Science* **272**, 551–554 (1996).
11. Vanzetta, I. & Grinvald, A. *Science* **286**, 1555–1558 (1999).
12. Logothetis, N. K., Guggenberger, H., Peled, S. & Pauls, J. *Nat. Neurosci.* **2**, 555–562 (1999).
13. Hu, X., Le, T. H & Ugurbil, K. *Magn. Reson. Med.* **37**, 877–884 (1997).
14. Engel, S. A., Glover, G. H. & Wandell, B. A. *Cereb. Cortex* **7**, 181–192 (1997).
15. Menon, R. S., Ogawa, S., Strupp, J. P. & Ugurbil, K. *J. Neurophysiol.* **77**, 2780–2787 (1997).